# Active damping control of higher-order resonance mode in positioning systems Application to prototype compliant dual positioning stage

Dee, N.J.; Natu, A.M.; HosseinNia, S.H.

**DOI**
10.1016/j.mechatronics.2025.103315

**Publication date**
2025

**Document Version**
Final published version

**Published in**
Mechatronics

Mechatronics 109 (2025) 103315

Contents lists available at ScienceDirect

Mechatronics

journal homepage: www.elsevier.com/locate/mechatronics

# Active damping control of higher-order resonance mode in positioning systems: Application to prototype compliant dual positioning stage

N.J. Dee, A.M. Natu *, S.H. HosseinNia

*Department of Precision and Microsystems Engineering, Delft University of Technology, Mekelweg 2, 2628 CD, Delft, The Netherlands*

ARTICLE INFO

*Keywords:*
Active damping control
High-pass filter
Higher-order
PPF
PID
Positioning stage
Non-collocated
Robustness

ABSTRACT

In precision positioning systems, lightly damped higher-order resonance modes can induce undesirable vibrations that degrade system performance and accuracy. These resonances pose additional challenges in non-collocated dual-stage positioning systems, where they significantly limit control bandwidth. Although conventional notch filters are commonly used alongside tracking controllers to enhance bandwidth, they lack robustness when faced with system parameter uncertainties. Moreover, the effects of the delimiting resonance on disturbance rejection remain. Active damping control has been successfully used to mitigate issues related to the primary resonance mode, but its application to higher-order modes has not been explored. This paper introduces a novel control strategy, High-Pass Positive Position Feedback (HP-PPF), inspired by existing methods but designed specifically for active damping of higher-order, non-collocated modes in positioning systems. The proposed method incorporates a second-order high-pass filter within a positive feedback loop, effectively attenuating the delimiting resonance. Integrated with a PID tracking controller in a dual-loop configuration, this method enhances disturbance rejection and robustness against model uncertainties, overcoming limitations of traditional notch filter-based methods while achieving comparable bandwidth improvements. The proposed control architecture is validated through a proof-of-concept experimental setup that demonstrates the effectiveness of the underlying mathematical framework.

## 1. Introduction

The high-tech industry experiences an ever-increasing demand for improved performance of motion stages, particularly in terms of accuracy and speed. This demand encompasses diverse high-precision applications like scanning-probe microscopy [1], micromanipulators [2], nanomanufacturing [3] and precision optics [4]. These stages require nanometre-level positioning accuracy, high response speed, compact structures, and large travel ranges [5]. The bandwidth of the control architecture driving the motion stages directly affects its speed and accuracy, with increasing bandwidth typically leading to improved performance [6]. However, increasing bandwidth comes with trade-offs, especially in linear control systems, where the waterbed effect limits performance enhancements. In addition, higher-order vibration modes in positioning systems introduce further constraints, as they generate unwanted vibrations when excited by high-frequency reference or disturbance signals [6,7]. In non-collocated dual-stage systems, these higher-order resonances impose additional restrictions on the control bandwidth, as the minimum-phase behaviour of non-collocated dynamics limits achievable bandwidth to a fraction of the higher-order resonance frequency [8].

Approaches such as feedforward [9], input shaping [10], inversion [11], and the application of notch filters [12,13] have successfully been employed in combination with conventional tracking controllers to mitigate the effects of parasitic resonances. Despite their potential effectiveness in systems with precise models and known references, these methods lack robustness against system parameter uncertainties and external disturbances [14]. Moreover, while notch filters, when used alongside tracking controllers can enable higher control bandwidths, which in turn improves the rejection of low-frequency disturbances, such as floor vibrations, the effects of the delimiting resonance still degrade the closed-loop disturbance rejection performance [15]. This residual effect can result in errors, particularly in multiple degree-of-freedom (DOF) systems, where cross-couplings may introduce disturbances near the resonance frequency, further degrading system performance.

Active damping control provides an alternative approach to addressing resonant modes by employing robust, fixed-structure feedback compensators that are straightforward to tune and rely on general system dynamics knowledge [16]. Compared to modal control or optimal controllers such as $H_\infty$-control, they provide a more practical

* Corresponding author.
*E-mail address:* A.M.Natu@tudelft.nl (A.M. Natu).

https://doi.org/10.1016/j.mechatronics.2025.103315
Received 28 November 2024; Received in revised form 17 March 2025; Accepted 3 April 2025
Available online 5 May 2025

and easier-to-implement solution. Modal control decomposes system dynamics with higher-order modes into modal signals, facilitating the implementation of existing active damping strategies [17]. However, its performance is sensitive to uncertainties in modal properties [18] and closely spaced modes further complicate control, potentially exciting unintended modes [19]. Moreover, precise sensor and actuator placement is essential, adding significant complexity to the implementation. Many robust feedback damping control schemes based on advanced optimal control theory have been developed to address the challenges posed by lightly damped resonant modes and system uncertainties, such as robust $H_\infty$-control [20]. While these synthesized damping controllers demonstrate excellent performance in the presence of uncertainties, their high-order transfer functions introduce significant complexity, making them less suitable for applications requiring high sampling rates, low computational cost, and efficient hardware implementation [21].

Common fixed-structure active damping controllers include direct velocity feedback (DVF) [22], integral resonance control (IRC) [23], integral force feedback (IFF) [24], negative position feedback (NPF) [25], positive position feedback (PPF) [26], positive velocity and position feedback (PVPF) [27], and positive acceleration, velocity and position feedback (PAVPF) [28]. Among these, PPF, PVPF, and PAVPF are widely adopted due to their ease of implementation, effective roll-off characteristics, ability to suppress multiple modes [29], and robustness against parameter variations [30]. However, PPF and PVPF require collocated actuator–sensor configurations because they are designed specifically for second-order systems [31]. Third-order models, which describe the dynamics of nanopositioning stages [32], have led to the development of the PAVPF damping controller, proven effective in enhancing bandwidth when combined with tracking control [31]. All these active damping controllers are guaranteed to be stable if and only if the open-loop gain at zero frequency is strictly less than one [33]. However, for non-collocated higher-order modes, this condition cannot be satisfied using existing methods due to their inherent gain-phase characteristics at lower frequencies.

Current fixed-structure active dampingmethods mainly focus on damping the primary resonance mode, typically assuming that higher-order modes are far enough away to be considered negligible and unlikely to induce vibrations and errors. However, these higher-order modes can show at relatively low frequencies in vicinity of the dominant mode, for example in systems incorporating flexure-based guiding mechanisms, where they contribute to errors when being excited. In industrial applications such as dual-stage positioning systems, including wafer and reticle stages in lithography machines [34], the influence of higher-order modes presents a critical challenge to performance and precision. Furthermore, non-collocated higher-order modes not only introduce positioning errors but also directly limit the control bandwidth.

Research has explored the concept of overactuation, which involves employing more actuators than there are rigid body modes to be controlled, to achieve active damping of higher-order modes [15]. However, this approach requires additional actuators and sensors, which might not always be feasible in practical applications and adds complexity to the system and its control architecture.

At present, no generally applicable fixed-structure active damping control strategy specifically addresses higher-order delimiting resonance modes, which limit positioning accuracy and, in certain applications, even tracking control bandwidth.

### 1.1. Contributions

This paper introduces a novel active damping control strategy inspired by existing methods, targeting the first dominant higher-order mode in positioning systems while maintaining the simplicity of a single-input single-output configuration. The focus is on mitigating the non-collocated higher-order mode in dual-stage positioning systems, which also restricts control bandwidth, by employing a low-order fixed-structure controller with clear tuning guidelines for straightforward implementation. The proposed framework, however, is adaptable for active damping of any higher-order mode causing undesirable vibrations in various systems. The key contributions of this work are as follows:

(1) This paper provides a general solution for active damping of higher-order delimiting modes, enhancing disturbance rejection at those frequencies.

(2) The proposed solution demonstrates robust performance against model uncertainties, particularly concerning resonance frequency variations within a defined range, offering significant improvements in robustness compared to a notch filter-based method.

(3) The novel active damping control method enhances control bandwidth when combined with conventional tracking controllers in dual-stage positioning systems, achieving comparable tracking performance to a notch filter-based method.

This paper is organized as follows: Section 2 presents an overview of the experimental setup used as a proof-of-concept and the governing system dynamics. Section 3 introduces the proposed active damping controller designed to address higher-order delimiting resonance modes. Section 4 details the integration of the active damping controller into a motion control loop for application in a dual-stage positioning system. Section 5 presents an experimental comparison between the novel active damping control and a notch filter-based solution, focusing on process disturbance and robustness against model uncertainties. Finally, conclusions are drawn in Section 6.

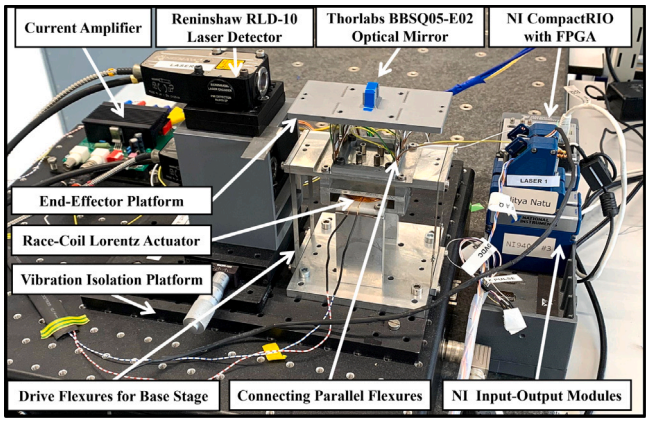


**Fig. 1.** Experimental setup.

## 2. System description

### 2.1. Proof-of-concept experimental setup

The experimental setup described in this paper is the single-axis dual-stage compliant micro-motion system from [15], illustrated in Fig. 1. This prototype serves as a proof-of-concept for a non-collocated dual-stage positioning system to validate the contributions of this work.

The system features a base and end-effector stage connected by parallel guiding flexures, with a second set of flexures linking the base to a fixed ground for translational movement while limiting other DOFs. Mounted on a vibration isolation platform to reduce external disturbances, the base stage is actuated by a race-coil Lorentz actuator, which produces a bidirectional force proportional to the input current. Input voltage signals are amplified and converted into the necessary current by a current amplifier, which maintains a constant gain factor during amplification up to a cutoff frequency of approximately 10 kHz. The position of the end-effector is measured using a laser interferometer,

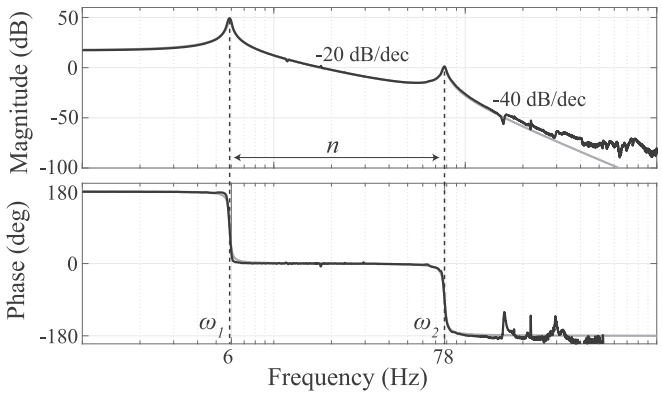


**Fig. 2.** Identified frequency response of experimental setup (black) and compensated analytical model of system dynamics (grey).

with a resolution of 39.5 nm, and an optical mirror, mounted on the end-effector stage to replicate the non-collocated dynamics.

For system identification, a sine sweep from 1 to 1000 Hz with increasing amplitude is applied to the Lorentz actuator, and the end-effector position is measured to estimate the transfer function based on input–output relations. Fig. 2 shows the identified frequency response and analytical model, with the first mode at 6 Hz and a dominant higher-order mode at 78 Hz. The analytical model's gain is adjusted for the stiffness of the bottom flexures, actuator, and amplifier dynamics, while the phase compensation corrects for a 180° offset from the operational amplifier's inversion.

### 2.2. System modelling

The dynamics of positioning systems are typically defined by a rigid-body mode, followed by one or more higher-order resonance modes. For the single-axis dual-stage positioning setup, the dynamics can be analytically modelled using a simplified double-mass–spring–damper system. This model effectively captures the behaviour of the first two dominant resonance modes. The non-collocated system dynamics, $G(s)$, represent the transfer function from the actuator force ($F_{\text{act}}$) to the displacement of the end-effector ($x_2$) and can be approximated by the following fourth-order transfer function to capture the two fundamental modes [15]:

$$G(s) = \frac{c_2 s + k_2}{(m_2 s^2 + c_2 s + k_2)(m_1 s^2 + (c_1 + c_2)s + (k_1 + k_2)) - (c_2 s + k_2)^2} \tag{1}$$

Here $m_1$ and $m_2$ represent the masses of the base stage and end-effector, while $k_1$, $c_1$ and $k_2$, $c_2$ represent the total stiffness and damping for the guiding and connecting flexures of the base and end-effector, respectively.

The non-collocated transfer function can be expressed in a general form, with the static gain determined by the stiffness $k_1$ normalized to one, as:

$$G(s) = \frac{{\omega_1}^2 {\omega_2}^2}{\left(s^2 + 2\zeta_1 \omega_1 s + {\omega_1}^2\right)\left(s^2 + 2\zeta_2 \omega_2 s + {\omega_2}^2\right)} \tag{2}$$

where $\omega_1$ and $\omega_2$ are the resonance frequencies with corresponding damping ratios $\zeta_1$ and $\zeta_2$ of the rigid-body mode and first higher-order mode, respectively. The spacing between the modes is denoted with $n$, such that $\omega_2/\omega_1 = n$, as indicated in Fig. 2. This mode spacing depends on the relative modal gains of the two resonance modes, which are governed by the stiffness and mass properties of the two stages, as described in Eq. (3).

$$n = \frac{\omega_2}{\omega_1} \approx \sqrt{\frac{k_2}{k_1}\frac{(m_1 + m_2)^2}{m_1 m_2}} \tag{3}$$

The non-collocated higher-order mode is characterized by a −20 dB/dec slope before and −40 dB/dec slope after resonance. The minimum phase behaviour is observed as a phase shift from −180° to −360° at the resonance frequency, corresponding to the magnitude slopes. The height of the delimiting resonance peak is approximately equal to $1/(2\zeta_2)$ [15], indicating that increasing the modal damping coefficient reduces the peak height in the frequency domain. In the following sections a methodology will be proposed to improve the damping characteristics of this mode through an active damping control feedback loop, effectively reducing the peak height of the undesired resonance mode.

## 3. Active damping using high-pass positive position feedback (HP-PPF)

The remainder of this paper focuses on the active damping of a non-collocated higher-order mode to fully illustrate the potential contributions. While the framework is applicable to any higher-order mode, the non-collocated mode presents specific challenges. In addition to generating unwanted vibrations, it also restricts the achievable control bandwidth. The minimum phase behaviour of a non-collocated mode inherently involves a −180° phase crossing at its resonance frequency. For stability, the non-collocated resonance peak in the open-loop response must remain below 0 dB. This requirement limits the gain that tracking controllers can apply, thereby constraining the achievable control bandwidth. Increasing the damping of this non-collocated higher-order mode is therefore of significant interest.

In contrast, the primary resonance mode is located below the control bandwidth and does not require additional damping, as its high gain is advantageous for motion control. A novel active damping control solution is proposed to address the undesired mode, which enhances damping properties and effectively reduces its peak height.

A simplified description of system dynamics in the region of interest ($\omega > \omega_1$), capturing the higher-order delimiting mode, is introduced as the following generalized transfer function:

$$G_p(s) = \frac{\omega_2^4}{s^2\left(s^2 + 2\zeta_2\omega_2 + \omega_2^2\right)} \quad \forall \quad \omega > \omega_1 \tag{4}$$

where $\omega_1$ is the primary resonance mode frequency, $\omega_2$ and $\zeta_2$ are the delimiting resonance mode frequency and corresponding damping ratio, respectively.

Active damping control of the primary mode is commonly achieved using various control techniques, such as employing a second-order low-pass filter within a positive feedback loop, as seen in PPF.

The frequency response of the non-collocated higher-order mode differs from that of the primary mode, showing a −20 dB/dec slope before resonance due to the influence of the rigid-body mode at lower frequencies, as illustrated in Fig. 2. The minimum phase behaviour of the non-collocated higher-order mode, which involves a phase shift from −180° to −360°, makes the direct implementation of active damping methods like PPF and NPF infeasible. These methods typically use second-order low-pass filters (LPF) and high-pass filters (HPF), with PPF employing positive feedback. Inverting the feedback sign in PPF effectively multiplies the open-loop response by −1, introducing a 180° phase shift, which can ensure a positive phase margin in the open-loop damping response, essential for stability as detailed in [16].

Fig. 3 presents the open-loop response of active damping control applied to the non-collocated higher-order mode described in Eq. (4), comparing second-order low-pass filter (LPF) and high-pass filter (HPF) used as damping controllers, with phase margins indicated. The 2nd-order LPF results in an open-loop phase between −180° and −360° (grey line), resulting in two negative phase margins. Positive feedback shifts the phase by 180°, which moves the phase from 0° to −360°, but the second crossover ($\varphi_{m2}$) remains unstable. Moreover, the LPF results in an open-loop gain exceeding one at frequencies below the target mode, which contradicts the gain requirement outlined in [16].

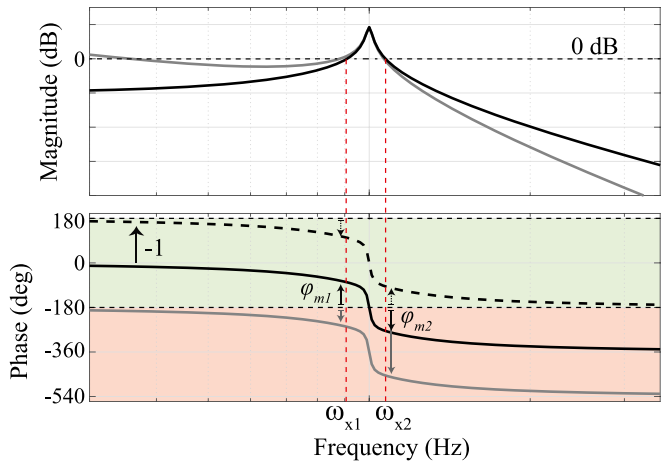


**Fig. 3.** Active damping open-loop ($(G_p(s) \cdot C_d(s))$ response; non-collocated higher-order mode with second-order LPF (grey) and second-order HPF (black) as damping controller. Positive feedback shifts phase with 180° (black dashed line) into stable region.

This requirement states that the open-loop gain must remain below one at frequencies both preceding and following the target mode to ensure the preservation of system dynamics.

To meet this requirement and maintain system stability, a second-order HPF is necessary. As illustrated in the magnitude response in Fig. 3 (black line), the HPF ensures that the open-loop gain remains below unity at lower frequencies. The HPF places the open-loop phase between 0° and −360° (solid black line), initially resulting in a negative phase margin at the second crossover. When positive feedback is applied, the phase shifts by 180° (black dashed line), bringing the open-loop phase into the stable region between 180° and −180°, thereby achieving positive phase margins at both crossovers. This open-loop gain and phase analysis demonstrates that only a second-order HPF within a positive feedback loop can achieve a stable closed-loop damping configuration for the non-collocated higher-order mode.

This analysis can be mathematically validated using the Routh–Hurwitz criterion to evaluate the stability of the closed damping loop. The characteristic equations for both the closed damping loops employing second-order HPF and LPF controllers, with positive and negative feedback signs, are given as follows:

$$
\begin{aligned}
&1 \pm G_p(s)C_{d-HPF}(s) = \\
&1 \pm \frac{\omega_2^4}{s^2(s^2+2\zeta_2\omega_2 s+\omega_2^2)} \frac{g_n s^2}{s^2+2\zeta_c\omega_2 s+\omega_2^2} = 0 \\
&s^4 + (2\zeta_c\omega_2 + 2\zeta_2\omega_2)s^3 + (2\omega_2^2 + 4\zeta_2\zeta_c\omega_2^2)s^2 + \cdots \\
&(2\zeta_2\omega_2^3 + 2\zeta_c\omega_2^3)s + (\omega_2^4 \pm g_n\omega_2^4) = 0
\end{aligned} \tag{5}
$$

$$
\begin{aligned}
&1 \pm G_p(s)C_{d-LPF}(s) = \\
&1 \pm \frac{\omega_4^2}{s^2(s^2+2\zeta_2\omega_2 s+\omega_2^2)} \frac{g_n}{s^2+2\zeta_c\omega_2 s+\omega_2^2} = 0 \\
&s^6 + 2\omega_2(\zeta_c+\zeta_2)s^5 + 2\omega_2^2(1+2\zeta_c\zeta_2)s^4 + \cdots \\
&2\omega_2^3(\zeta_c+\zeta_2)s^3 + \omega_2^4 + 0\cdot s \pm g_n\omega_2^4 = 0
\end{aligned} \tag{6}
$$

The Routh–Hurwitz criterion for stability requires all coefficients of the characteristic polynomial to be positive and nonzero. Table 1 summarizes these coefficients derived from the characteristic equations. Notably, when a second-order low-pass filter (LPF) is employed as the active damping controller, the coefficient $a_1$ is always zero, regardless of the feedback sign. This results in an unstable pole, which corresponds to the negative phase margin observed in Fig. 3.

In contrast, the second-order high-pass filter (HPF) shows that stable closed-loop behaviour can be achieved under certain feedback conditions. Specifically, stability holds with positive feedback if $1-g_n > 0$ and with negative feedback if $1+g_n > 0$. However, despite these conditions, the open-loop phase analysis for the negative feedback case shows instability. This discrepancy highlights that the necessary conditions provided by the Routh–Hurwitz criterion are insufficient on their own; the sufficient condition must also be satisfied to confirm stability.

**Table 1**
Coefficients of the characteristic equation for active damping of the non-collocated higher-order mode using a 2nd-order (2o) LPF and 2nd-order (2o) HPF with both positive and negative feedback signs.

| | 2o LPF (∓ Feedback) | 2o HPF (∓ Feedback) |
|---|---|---|
| $a_6$ | 1 | – |
| $a_5$ | $2\omega_2(\zeta_c+\zeta_2)$ | – |
| $a_4$ | $2\omega_2^2(1+2\zeta_c\zeta_2)$ | 1 |
| $a_3$ | $2\omega_2^3(\zeta_c+\zeta_2)$ | $2\omega_2(\zeta_c+\zeta_2)$ |
| $a_2$ | $\omega_2^4$ | $2\omega_2^2(1+2\zeta_c\zeta_2)$ |
| $a_1$ | **0** | $2\omega_2^3(\zeta_c+\zeta_2)$ |
| $a_0$ | $\pm g_n\omega_2^6$ | $\boldsymbol{\omega_2^4 \pm g_n\omega_2^4}$ |

**Table 2**
Coefficients of the first column of Routh array for active damping of the non-collocated higher-order mode using a 2nd-order HPF with both positive and negative feedback signs.

| | Negative feedback | Positive feedback |
|---|---|---|
| $a_4$ | 1 | 1 |
| $a_3$ | $2\omega_2(\zeta_2+\zeta_c)$ | $2\omega_2(\zeta_2+\zeta_c)$ |
| $b_1$ | $\omega_2^2(4\zeta_2\zeta_c+1)$ | $\omega_2^2(4\zeta_2\zeta_c+1)$ |
| $c_1$ | $-\frac{2\omega_2^3(g_n-4\zeta_2\zeta_c)(\zeta_2+\zeta_c)}{4\zeta_2\zeta_c+1}$ | $\frac{2\omega_2^3(g_n+4\zeta_2\zeta_c)(\zeta_2+\zeta_c)}{4\zeta_2\zeta_c+1}$ |
| $a_0$ | $\omega_2^4(g_n+1)$ | $\omega_2^4(1-g_n)$ |

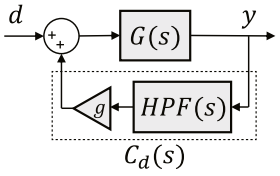


**Fig. 4.** Active damping control loop employing second-order high-pass filter (HPF) in positive feedback (HP-PPF).

Table 2 presents the first-column coefficients of the Routh array for the second-order HPF under both feedback cases. For the negative feedback loop, two sign changes in the first column indicate two right-half-plane poles, confirming instability. In contrast, for the positive feedback loop, all first-column coefficients remain of the same sign when $1-g_n > 0$, ensuring stability.

It is important to note that the negative feedback loop becomes stable when $g_n < 4\zeta_2\zeta_c$. However, given that the values of $\zeta_2$ and $\zeta_c$ are typically small, this condition would only be met when $g_n$ is very small. Since $g_n$ directly affects damping performance, a higher $g_n$ is usually required to achieve adequate peak attenuation. Consequently, in practical terms, only the positive feedback configuration of the second-order high-pass filter can achieve a stable closed-loop damping system.

Here we introduce a second-order high-pass filter in positive feedback (HP-PPF) utilized as an active damping controller, as visualized in Fig. 4. The closed-loop damping performance is tuned using gain parameter $g$, which for mathematical brevity is normalized to $g_n$, such that the open-loop response has unity gain, i.e. $\left|G_p(i\omega)\cdot g_n \cdot HPF(i\omega)\right|_{\omega=0} = 1$. The resulting HP-PPF controller is given by:

$$
C_d(s) = g_n \cdot \frac{s^2}{s^2+2\zeta_c\omega_c s+\omega_c^2} \tag{7}
$$

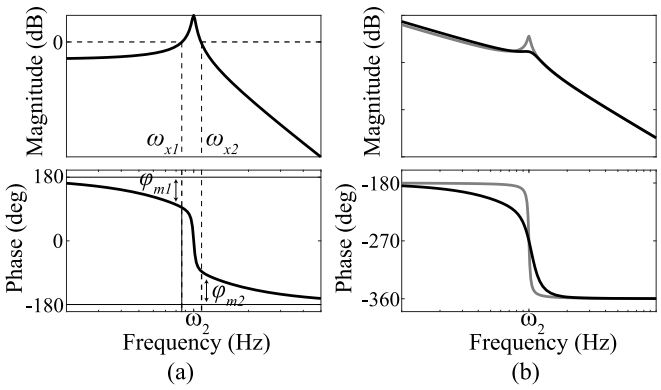


**Fig. 5.** HP-PPF active damping control (black) of non-collocated higher-order mode (grey) open-loop response (a) and closed-loop response (b).

where controller frequency $\omega_c$ equals the frequency of the higher-order resonance mode to be damped ($\omega_c = \omega_2$). The effective damping is then determined by the damping ratio $\zeta_c$ and the normalized feedback gain $g_n$ of the controller. The resulting closed damping loop is described by:

$$CL_d(s) = \frac{y}{d} = \frac{G_p(s)}{1 - G_p(s)C_d(s)}. \tag{8}$$

The magnitude of the non-collocated higher-order mode, in Eq. (4), at the resonance frequency $\omega_2$ can be calculated as:

$$\left|G_p(i\omega_2)\right| = \left|\frac{\omega_2^4}{-\omega_2^2(-\omega_2^2 + 2\zeta_2\omega_2^2 i + \omega_2^2)}\right| = \frac{1}{2\zeta_2} \tag{9}$$

The magnitude of the closed damping loop response, given in Eq. (8), at the resonance frequency, can be calculated in similar fashion as:

$$\left|CL_d(i\omega_2)\right| = \frac{2\zeta_c}{g_n + 4\zeta_c\zeta_2} = \frac{1}{2\left(\frac{g_n}{4\zeta_c} + \zeta_2\right)}, \tag{10}$$

From these expressions, it can be derived that the damping ratio of the closed damping loop can be described as:

$$\zeta_{CL_d} = \zeta_2 + \frac{g_n}{4\zeta_c}, \tag{11}$$

This demonstrates an increase in the effective closed-loop damping ratio when $g_n > 0$ and $\zeta_c > 0$, emphasizing the effectiveness of the HP-PPF controller in enhancing the damping characteristics of the non-collocated higher-order mode. Notably, this relationship holds specifically at the resonance frequency. While a combination of high gain ($g_n$) and low damping ($\zeta_c$) can reduce the magnitude at the exact resonance frequency, it also results in peak splitting. Peak splitting refers to the emergence of new peaks in the closed-loop frequency response, which occurs when the open-loop gain is close to one and has a phase of $\pm 180°$ [16]. When tuning $g_n$ and $\zeta_c$ the phase requirements outlined in [16] should be taken into account.

The open-loop response depicted in Fig. 5(a) shows the resulting phase margins ($\varphi_{m1}, \varphi_{m2}$) at both crossover frequencies ($\omega_{x1}, \omega_{x2}$) respectively, which can be tuned with control parameter $\zeta_c$. Meanwhile, the closed-loop response shown in Fig. 5(b) demonstrates the attenuation of the non-collocated resonance peak with the proposed HP-PPF active damping control architecture. Following the characteristic equation in Eq. (5), the Routh–Hurwitz stability criterion indicates that the damping loop using HP-PPF is stable when the condition $0 < g_n < 1$ is satisfied.

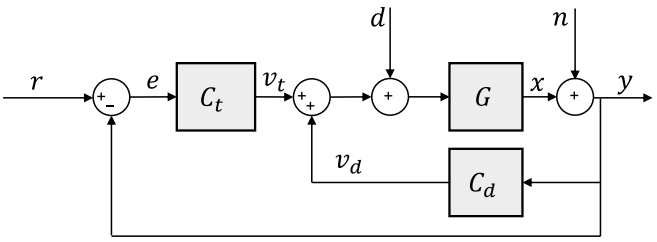


**Fig. 6.** Dual-loop architecture incorporating motion control and active damping control.

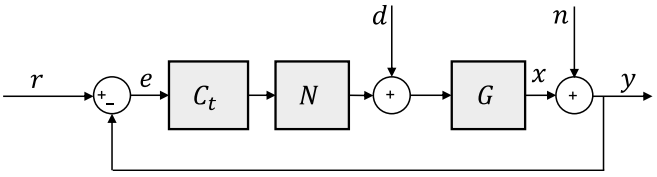


**Fig. 7.** Control architecture incorporating motion control and notch filter.

## 4. Active damping control of dual-stage positioning systems

### 4.1. Combining active damping control and motion control

The previous section showed that the HP-PPF active damping controller effectively attenuates higher-order modes, applicable to a single-axis dual-stage positioning system. This paper focuses on using this method in two DOF positioning systems as a case study, with dynamics described by Eq. (2). The adaptable solution also addresses higher-order system modes. A dual-loop control architecture, combining motion and active damping control as shown in Fig. 6, is used for damping and tracking control [31,35].

The control architecture features two distinct loops: an outer feedback loop utilizing a tracking controller ($C_t(s)$), typically a tamed PID controller, to achieve accurate motion tracking, and an inner feedback loop that incorporates an active damping controller ($C_d(s)$). In the proposed HP-PPF solution, the inner loop uses a second-order high-pass filter within a positive feedback configuration to actively dampen the higher-order delimiting mode. The dual-stage positioning system ($G(s)$) is represented by the transfer function in Eq. (2). The dual closed-loop transfer function is given by:

$$CL(s) = \frac{G(s)C_t(s)}{1 + G(s)\left(C_t(s) - C_d(s)\right)} \tag{12}$$

where the inner closed damping loop is described by Eq. (8). The standard tamed PID controller is defined as follows:

$$C_{PID}(s) = k_p\underbrace{\left(1 + \frac{\omega_i}{s}\right)}_{\text{Integrator}}\underbrace{\left(\frac{1 + s/\omega_d}{1 + s/\omega_t}\right)}_{\text{Lead/Lag}}\underbrace{\left(\frac{\omega_l}{s + \omega_l}\right)}_{\text{LPF}} \tag{13}$$

The PID controller includes a low-pass filter (LPF) to suppress high-frequency noise and unmodelled dynamics. The various frequency bands are computed, in terms of open-loop crossover frequency $\omega_x$ (0 dB crossing), as outlined in [36].

$$\begin{aligned} &\omega_d = \frac{\omega_x}{3} \quad , \quad \omega_t = 3\omega_x \quad , \quad \omega_i = \frac{\omega_x}{10} \\ &\omega_l \geq 10\omega_x \quad , \quad k_p = 0.33\left|\frac{1}{G(i\omega_x)}\right| \end{aligned} \tag{14}$$

The PID tracking controller is designed to ensure stability and robustness by achieving sufficient gain margin (GM $\geq$ 6 dB) and phase margin (PM $\geq 30°$) in open-loop.

### 4.2. Stability of inner closed damping loop

Active damping is achieved in the inner loop of the dual-loop control architecture, as shown in Fig. 6. The stability of the active damping loop was previously analysed for the simplified system $G_p(s)$, where the rigid-body mode was neglected. However, in the dual-stage positioning system, the dynamics are governed by the fourth-order transfer function in Eq. (2), where the rigid-body mode cannot be ignored. This suggests that the stability condition of the inner active damping loop, derived earlier, may be affected by the presence of the rigid-body mode.

The characteristic equation of the inner closed damping loop, considering the fourth-order system dynamics and HP-PPF controller, is given as follows:

$$\begin{aligned}&s^6+\left[2\omega_1\left(\zeta_1+\zeta_2 n+\zeta_c n\right)\right]s^5+\\&\left[\omega_1^2\left(1+2n^2+4\zeta_1\zeta_2 n+4\zeta_1\zeta_c n+4\zeta_2\zeta_c n^2\right)\right]s^4+\\&\left[2n\omega_1^3\left(2\zeta_1 n+\zeta_2+2\zeta_c n^2+4\zeta_1\zeta_2\zeta_c n+\zeta_2 n^2\right)\right]s^3+\\&\left[n^2\omega_1^4\left(2+4\zeta_1\zeta_c n+4\zeta_2\zeta_c+n^2+4\zeta_1\zeta_2 n-g_n\right)\right]s^2+\\&\left[2n^3\omega_1^5\left(\zeta_c+\zeta_1 n+\zeta_2\right)\right]s+\left[n^4\omega_1^6\right]=0\end{aligned} \tag{15}$$

Based on the necessary condition from the Routh–Hurwitz criterion for closed-loop stability, the following condition emerges:

$$0<g_n<\underbrace{4\,\zeta_2\,\zeta_c+n^2+4\,n\,\zeta_1\,\zeta_2+4\,n\,\zeta_1\,\zeta_c+2}_{\mathrm{k}} \tag{16}$$

The factor $k$ can be approximated as $k\approx n^2+2$ due to the typically small values of $\zeta_1,\zeta_2$ and $\zeta_c$. This factor compensates for modal gain variations, which spaces modes further apart. The spacing between the modes ($n$) is directly related to the gain of the higher-order mode relative to the primary mode.

According to the gain criterion outlined in [16], the open-loop gain of the active damping loop must peak above 0 dB as indicated in Fig. 5(a), introducing two crossover frequencies to reduce sensitivity at resonance and therewith enhance the damping characteristics of the mode. For further separated modes, the relatively lower modal gain of the higher-order mode necessitates a higher gain in the damping controller ($g_n$), which is essentially described by factor $k$, to meet this criterion for effective active damping. To simplify the formulation, the gain of the active damping controller is adjusted to account for this modal gain dependency, such that $g_k=g_n/k$, resulting in the following expression for the active damping controller:

$$C_d(s)=g_k\cdot\frac{s^2}{s^2+2\zeta_c\omega_c s+\omega_c^2} \tag{17}$$

Upon re-evaluation of the characteristic equation with compensated gain $g_k$, a necessary stability condition for the damping loop emerges as $0<g_k<1$, independent of $n$. This condition underscores the role of $k$ in compensating for the modal gain difference.

However, even with the inclusion of $k\approx n^2+2$ in the HP-PPF controller, the stability of the inner damping loop remains influenced by the spacing between the two modes. The open-loop responses in Fig. 8 illustrate the application of the same HP-PPF controller, which satisfies the condition in Eq. (16), to two systems with different mode spacing. In this example, the active damping controller achieves a stable closed damping loop when $n=25$ (Fig. 8(a)), but leads to an unstable closed damping loop when $n=15$ (Fig. 8(b)). This illustrates that closer spacing between the rigid-body and higher-order mode increases the likelihood of destabilizing the inner damping loop.

The root-locus plot in Fig. 9 illustrates that the closed-loop poles associated with the first resonance mode ($\omega_1$) in the right-half-plane (RHP) shift to more negative real values as $n$ increases, retaining stability of the inner closed-loop system, as those system poles initially lie in the RHP. This indicates that when the modes are closely spaced, the active damping controller can destabilize the closed-loop poles of the first resonance mode. The larger angle between the real axis and

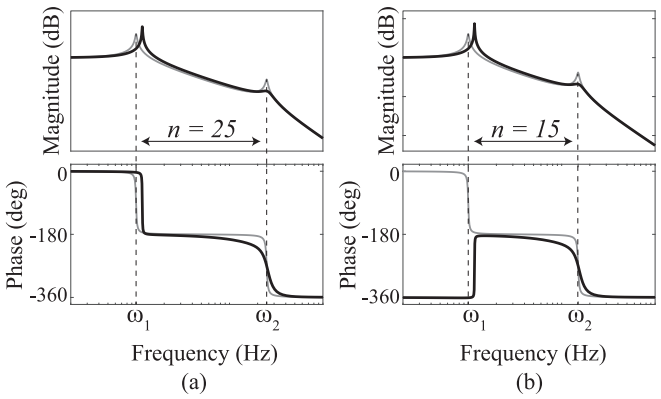


**Fig. 8.** Closed inner active damping loop using same HP-PPF controller is stable when mode spacing $n=25$ (a) and unstable when $n=15$ (b).

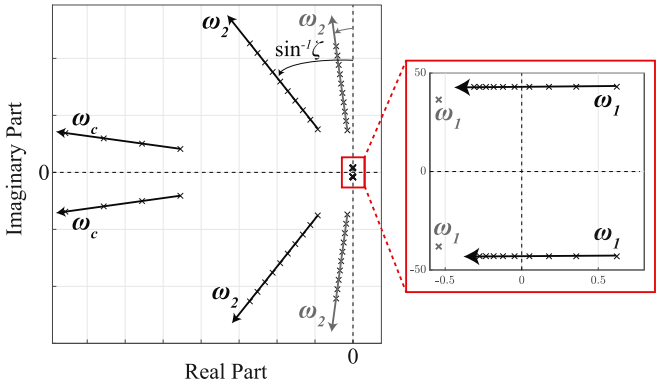


**Fig. 9.** Trajectories of closed damping loop poles (black) and system poles (grey) for increasing values of $n$.

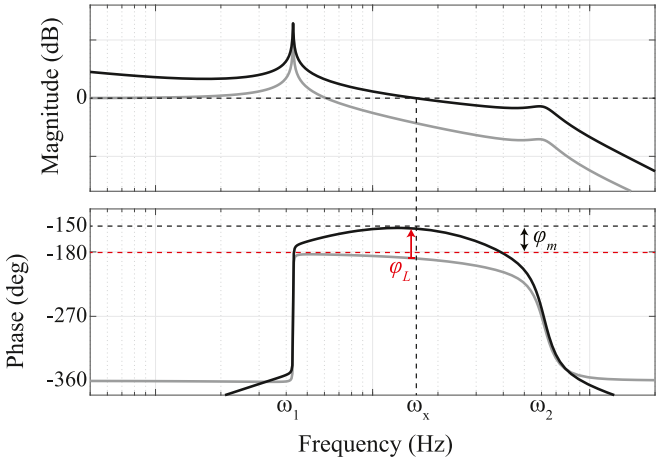


**Fig. 10.** Added phase at crossover in open-loop response $C_t(s)\cdot CL_d(s)$ (black), representing PID controller combined with the unstable inner damping loop (grey).

the closed-loop pole trajectories corresponding to the second mode ($\omega_2$) reflects an increase in the damping ratio of this mode. Note that this angle, and consequently the damping ratio, remains constant as $n$ varies.

The instability of the inner damping loop is not a significant concern, as tracking controllers, such as PID controllers, are commonly used in motion control to stabilize otherwise unstable systems [37]. Similarly, in cases where the inner active damping loop becomes unstable due to closely spaced resonance modes, a PID controller can

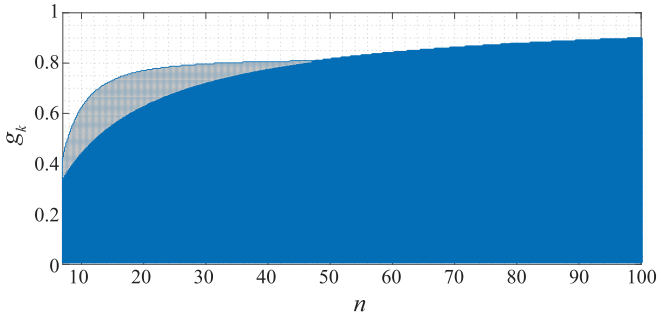


**Fig. 11.** Stability regions as a function of $g_k$ and $n$ ($\zeta_c = 0.3$), indicating where both the inner damping loop and outer closed-loop are stable (blue), and the region where the inner damping loop is unstable but the outer closed-loop with the PID tracking controller becomes stable (grey).

stabilize the system by shifting the unstable poles to the left-half-plane. In the frequency domain, this stabilization can be visualized through the derivative (D) action of the PID controller, which introduces an additional phase lead at the crossover frequency [37]. This phase lead effectively raises the phase above −180° at crossover, ensuring system stability and providing sufficient phase margin. The outer open-loop response in Fig. 10 of the control architecture in Fig. 6, represented by $C_t(s) \cdot CL_d(s)$, where $C_t(s) = C_{PID}(s)$ as defined in Eq. (13), demonstrates how a standard tamed PID controller adds phase lead ($\varphi_L$) at crossover ($\omega_x$), retaining stability of the outer closed-loop system and ensuring a phase margin ($\varphi_m$) of approximately 30°.

Fig. 11 illustrates the stability of both the inner damping loop and the outer closed-loop with the PID tracking controller, as a function of the HP-PPF controller feedback gain ($g_k$) and the mode spacing ($n$). The blue region represents combinations of $g_k$ and $n$ where the inner closed damping loop remains stable. In contrast, the grey region indicates where the inner closed-loop is unstable, but the PID controller, when properly tuned to introduce phase lead at crossover according to the design rules in Eq. (14), stabilizes the overall closed-loop system. As $n$ increases, the stable region converges towards $g_k = 1$, in line with the derived Routh–Hurwitz stability condition. It is important to note that this plot assumes a fixed damping control parameter $\zeta_c$ set to 0.3, and the PID controller is tuned based on standard rules-of-thumb (Eq. (14)).

### 4.3. Control parameter tuning

The dual closed-loop system's performance mainly depends on the three control parameters of the HP-PPF controller $g_k$, $\zeta_c$, and the PID controller's desired crossover frequency (Eq. (14)). The second-order high-pass filter's cut-off frequency ($\omega_c$) in HP-PPF is tuned to damp the mode at 78 Hz in the experiment. Increasing the damping of the controller ($\zeta_c$) leads to greater peak attenuation and robustness, however, this comes at the cost of increased phase lag, which limits the maximum achievable control bandwidth. Similarly, increasing the gain ($g_k$), within the stability limits dependent on $n$ (Fig. 11), improves peak attenuation but also increases process sensitivity at lower frequencies, as discussed in Section 5.1. Consequently, tuning the parameters involves a trade-off between peak attenuation, maximum control bandwidth, and low-frequency disturbance rejection. Simultaneous design of control parameters in a dual-loop architecture through optimization has proven significantly more effective than the sequential design of the damping controller and tracking controller [31].

$$\begin{aligned} \max_{\mathbf{x}} \quad & \omega_x = \left\{ \omega \middle| \left| L(\omega, \mathbf{x}) \right| = \left| C_t(\omega) \cdot CL_d(\omega, \mathbf{x}) \right| = 1 \right\} \\ \text{subject to} \quad & \frac{1}{2} \left| L(\omega, \mathbf{x}) \right|_{\omega=\omega_x} \Big| - 1 \geq 0 \\ & \frac{6}{\pi} \cdot \angle L(\omega, \mathbf{x}) \Big|_{\omega=\omega_x} - 1 \geq 0 \\ \text{and} \quad & 0 < g_k < 1 \\ & 0 < \zeta_c < 1 \\ & \omega_1 < \omega_x < \omega_2 \\ \text{where} \quad & \mathbf{x} = (g_k, \zeta_c, \omega_x)^T \end{aligned} \tag{18}$$

To simultaneously determine the control parameters for both the damping and tracking controller ($g_k$, $\zeta_c$, and $\omega_x$ respectively), a gradient-based optimization method utilizing the sequential quadratic programming (SQP) algorithm is employed [38]. The optimization aims to maximize the open-loop bandwidth (crossover frequency $\omega_x$) of the dual-loop, under the constraints of maintaining sufficient gain and phase margin. The optimization problem is formulated in Eq. (18).

The optimization process is employed to determine the control parameters that achieve maximum open-loop bandwidth for damping and tracking control of the identified frequency response of the experimental setup (Fig. 2). This results in $g_k = 0.2618$, $\zeta_c = 0.7185$ and $\omega_x = 25$ Hz.

### 4.4. Attenuating feedback noise using band-pass filter

The high-pass active damping controller lacks roll-off beyond its cut-off frequency, which can amplify high-frequency noise present in practical applications. This noise amplification increases power demands, potentially causing the amplifier to overheat, saturate, or produce distorted output, ultimately degrading system performance and lifespan.

Mathematically, the signal entering the amplifier through the inner feedback loop can be represented as:

$$\frac{v_d}{n} = \frac{C_d(s)}{1 + C_d(s)G(s)} \tag{19}$$

which simplifies to $\frac{v_d}{n} \approx C_d(s)$ at high frequencies due to the system roll-off ($\lim_{s\to\infty} G(s) = 0$). In this high-frequency range, where noise dominates, the noise entering the amplifier through the inner feedback loop can be expressed as:

$$v_d = \lim_{s\to\infty} C_d(s) \cdot n \approx g_k \cdot n \tag{20}$$

This emphasizes the importance of high-frequency roll-off in the damping controller to reduce the magnitude of the high-frequency component of the transfer function.

To address this issue, a low-pass filter can be introduced, which provides high-frequency roll-off and effectively transforms the damping controller into a band-pass filter, as illustrated in Fig. 12 for the case where the width of the band-pass $\alpha$ is set to 10. Depending on the required high-frequency roll-off, a higher-order low-pass filter may be utilized.

The band-pass active damping controller can be mathematically represented as follows:

$$C_d(s) = g_k \cdot \frac{s^2}{s^2 + 2\zeta_c\omega_c s + \omega_c^2} \cdot \left( \frac{\omega_L}{s + \omega_L} \right)^m \tag{21}$$

where $m$ denotes the order of the low-pass filter, and $\omega_L = \alpha \cdot \omega_c$.

However, placing a low-pass filter too close to the high-pass filter of the HP-PPF controller can adversely affect the effective damping performance. This relative distance between the individual cut-off frequencies is described by the width of the resulting band-pass filter, denoted by $\alpha$.

The magnitude reduction of the inner closed damping loop at resonance frequency is evidenced in Eq. (10). When a second-order

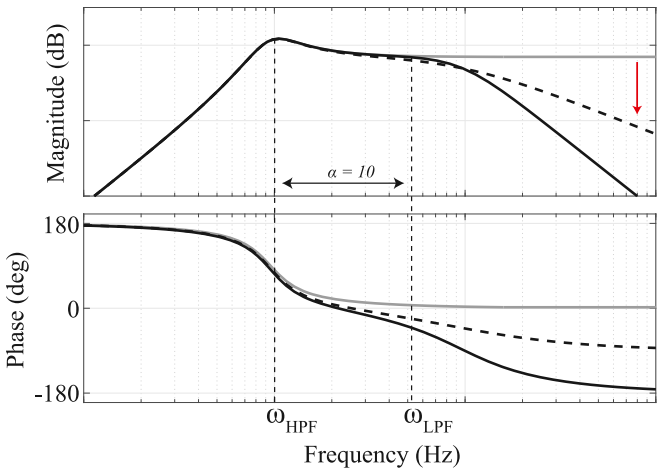


**Fig. 12.** Second-order HPF (grey) with added first-order LPF (black-dotted) and second-order LPF (black).

low-pass filter (LPF) is incorporated into the active damping controller for noise attenuation, the active damping controller is represented by Eq. (21), with $m = 2$, $\omega_L = \alpha \cdot \omega_c$, neglecting the damping ratio of the LPF for mathematical simplicity. The magnitude of the closed-loop damping response at the resonance frequency, considering only the contribution of the higher-order mode for mathematical simplicity as expressed in Eq. (4), can be determined as:

$$\left|CL_{d-BPF}(i\omega_2)\right| = \frac{2\zeta_c \left|\alpha^2 + 1\right|}{\left|\alpha^2 g_n - 4\zeta_c\zeta_2 + 4\alpha^2\zeta_c\zeta_2\right|} \tag{22}$$

This equation illustrates the dependence of damping effectiveness on the width parameter $\alpha$ of the band-pass filter. Assuming $\alpha \gg 1$, the expression simplifies to:

$$\left|CL_{d-BPF}(i\omega_2)\right| = \frac{2\zeta_c|\alpha^2|}{|\alpha^2 g_n + 4\alpha^2\zeta_c\zeta_2|} \approx \frac{1}{2\left(\frac{g_n}{4\zeta_c} + \zeta_2\right)} \tag{23}$$

The similarity with Eq. (10) suggests that when the low-pass filter (LPF) is sufficiently far from the high-pass filter (HPF), the active damping is unaffected. However, if the LPF is positioned too close to the HPF, the magnitude reduction is influenced. Therefore, careful tuning of the LPF frequency is essential, balancing damping performance with high-frequency noise attenuation. In the presented application, $\alpha$ is set to 10 to maintain the primary objective of unaffected damping performance. For the proper tuning of $\alpha$, methods such as dynamic error budgeting can be utilized [39].

## 5. Experimental implementation

The proposed HP-PPF active damping controller, optimized for the experimental setup with an added low-pass filter for noise attenuation, is implemented in real-time through discretization using the Tustin method. The chosen parameters, designed to maximize open-loop bandwidth, lead to an unstable inner damping loop due to closely spaced modes. The introduced tamed PID controller stabilizes the outer closed-loop system. Through closed-loop system identification, the frequency response of the inner damping loop is isolated, which is illustrated in Fig. 13. The results demonstrate a significant reduction (~ 16 dB) of the resonance peak. The primary resonance mode $\omega_1$ is shifted from 6 Hz to 7.5 Hz in the closed damping loop response, yet it remains sufficiently below the crossover frequency $\omega_x$.

An experimental comparison is conducted to showcase the benefits of implementing HP-PPF active damping control across three scenarios. In each case, the controllers are designed to maximize open-loop bandwidth while ensuring stability and robustness margins. The performance of these scenarios will be compared and assessed throughout the remainder of the paper.

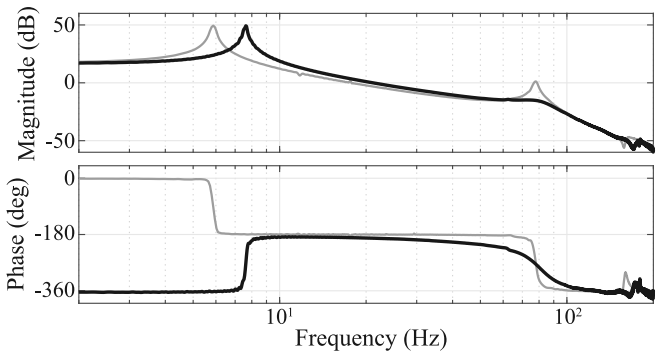


**Fig. 13.** Experimentally identified inner closed damping loop $CL_d$ (black) and identified frequency response of experimental setup (grey).

**Table 3**
Control parameters, open-loop bandwidth ($\omega_x$) and corresponding margins (GM, PM) for three cases.

| | Control parameters | $\omega_x$ | GM | PM |
|---|---|---|---|---|
| Case A | – | 12 Hz | 13 dB | 37° |
| Case B | $Q = 7$, $\zeta_N = 0.15$ | 22 Hz | 6 dB | 30° |
| Case C | $g_k = 0.26$, $\zeta_c = 0.71$ | 25 Hz | 6 dB | 30° |

Case A (PID): Only a tamed PID controller ($(C_t(s))$) is employed for tracking control, leaving the delimiting resonance undamped. This configuration yields a maximum open-loop bandwidth of 12 Hz, limited by the non-collocated higher-order resonance.

Case B (PID + Notch): A conventional notch filter ($N(s)$), described in Eq. (24), is introduced, following the control architecture in Fig. 7.

$$N(s) = \frac{s^2 + (2\zeta_N/Q)s + \omega_N^2}{s^2 + 2\zeta_N s + \omega_N^2} \tag{24}$$

The notch filter is tuned to reduce the delimiting resonance peak to a level comparable to that of the active damping controller with similar phase lag, resulting in a maximum open-loop bandwidth of 22 Hz.

Case C (PID + Active Damping): The dual-loop architecture shown in Fig. 6 incorporates the optimized HP-PPF controller and tamed PID controller, achieving an open-loop bandwidth of 25 Hz.

The tuned control parameters, resulting open-loop bandwidths and stability margins for the three cases are presented in Table 3. The corresponding experimental open-loop frequency responses are shown in Fig. 14. This comparison illustrates that the HP-PPF active damping control architecture can achieve open-loop bandwidths and stability margins comparable to those of an industry-standard notch filter-based solution.

### 5.1. Disturbance rejection

The previous section demonstrated the practical implementation of the proposed active damping control method, showcasing its ability to achieve control bandwidth improvements comparable to industry-standard notch filters. However, the primary objective of this novel approach is not to exceed the bandwidth of existing solutions but to address the inherent limitations of notch filters. While notch filters effectively suppress resonance in closed-loop responses, their ability to improve disturbance rejection is limited, as the delimiting resonance remains noticeable in the closed-loop disturbance rejection [15].

The dual closed-loop process sensitivity function when implementing active damping control, $PS_{ADC}(s)$, can be determined by:

$$PS_{ADC}(s) = \frac{y}{d} = \frac{G(s)}{1 + G(C_t(s) - C_d(s))} = \frac{G_d(s)}{1 + G_d(s)C_t(s)} \tag{25}$$

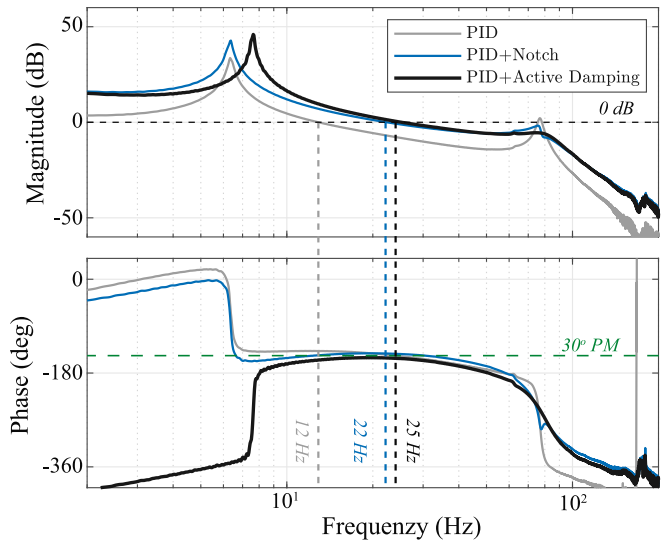


**Fig. 14.** Experimentally identified open-loop response indicating 0 dB crossover frequencies for three comparison cases.

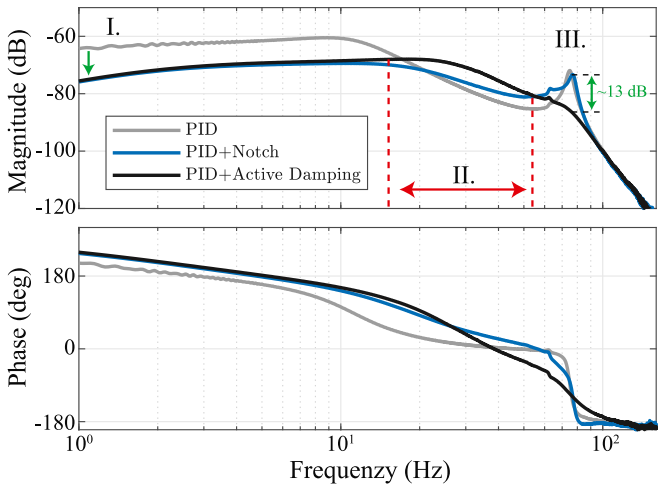


**Fig. 15.** Experimentally identified closed-loop process sensitivity responses for three comparison cases.

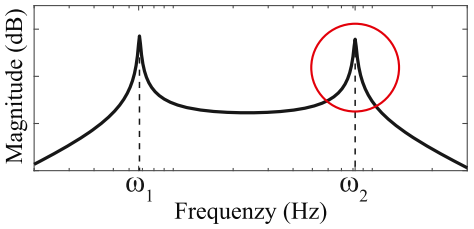


**Fig. 16.** Magnitude of cross-coupling frequency response $x_2/F_1$ in multi-DOF positioning system; transfer function from actuator at $m_1$ to position of $m_2$.

Here, the inner active damping loop from Eq. (8) is represented by an equivalent plant ($G_d(s)$), incorporating the damped delimiting mode. In practice, a notch filter ($N(s)$) can be implemented to obtain similar peak attenuating in the open-loop around the frequency of the higher-order mode ($\omega_2$) and thus:

$$|G_d(i\omega)| = \left|\frac{G(i\omega)}{1 - G(i\omega)C_d(i\omega)}\right| = |G(i\omega)\cdot N(i\omega)|\Big|_{\omega=\omega_2} \tag{26}$$

The closed-loop process sensitivity when using the notch filter, denoted as $PS_N(s)$, can be calculated as follows:

$$PS_N(s) = \frac{G(s)}{1 + G(s)NC_t(s)} \tag{27}$$

Combining Eqs. (26) and (27) gives:

$$|PS_N(i\omega)| \approx \left|\frac{G(i\omega)}{1 + G_d(i\omega)C_t(i\omega)}\right|_{\omega=\omega_2} \tag{28}$$

The ratio of the two process sensitivity functions can be expressed as:

$$\begin{aligned}\frac{|PS_{ADC}(s)|}{|PS_N(s)|} &= \left|\frac{G_d(s)}{1 + G_d(s)C_t(s)}\right| \Big/ \left|\frac{G(s)}{1 + G_d(s)C_t(s)}\right| \\ &= \frac{|G_d(s)|}{|G(s)|} \approx \frac{|G(s)\cdot N(s)|}{|G(s)|} = |N(i\omega)|_{\omega=\omega_2} = \frac{1}{Q} < 1\end{aligned} \tag{29}$$

This demonstrates that the implementation of active damping control results in a reduced process sensitivity around the frequency of the higher-order delimiting mode, indicating better disturbance rejection, which is not achieved when using a notch filter.

This reduction around the delimiting resonance is clearly observed in the experimentally obtained process sensitivity frequency responses in Fig. 15 (III.), where the delimiting resonance peak remains present when a notch filter is employed. At low frequencies (I.), both the active damping control architecture and notch filter architecture reduce the process sensitivity due to the higher gains of the tracking controllers.

The active damping architecture demonstrates significantly reduced process sensitivity around the frequency of the delimiting mode, compared to the notch filter architecture. In multi-DOF positioning stages that use multiple actuators and sensors, actuation in one DOF can introduce disturbances into the other DOF of the system, particularly at this delimiting mode frequency ($\omega_2$). This effect is evident in the cross-coupling transfer function of a multi-DOF positioning system, as illustrated in Fig. 16.

To replicate such cross-coupling disturbance, a multisine signal, composed of frequencies around the delimiting mode, is applied as a process disturbance to the closed-loop system. This multisine signal includes components at 76 Hz and 80 Hz to illustrate the system's ability to reject disturbances at frequencies close to the delimiting mode. The multisine disturbance signal $d(t)$ can be expressed as:

$$d(t) = A\sin(2\pi\cdot 76t) + A\sin(2\pi\cdot 80t) \tag{30}$$

where $A$ represents the amplitude of the sine waves. The resulting output response, normalized with the input amplitude $A$, depicted in Fig. 17, clearly illustrates the superior disturbance rejection achieved with the implementation of active damping control. Similarly, in Fig. 18 when a chirp signal is applied as a disturbance input, an improvement in signal rejection is observed around the frequency of the delimiting mode.

The proposed HP-PPF active damping control architecture demonstrates superior disturbance rejection around the frequency of the higher-order delimiting mode compared to the notch filter-based solution. However, as shown in Fig. 15 (II.), there is an increase in the magnitude of the process sensitivity function in the frequency range between the rigid-body mode ($\omega_1$) and the higher-order mode ($\omega_2$) when using active damping control. This increase is attributed to spillover effects within the inner damping loop, which can be mitigated by reducing the gain $g_k$ of the damping controller. Consequently, a trade-off arises between reducing the delimiting resonance peak and increasing process sensitivity in this lower frequency range. This suggests that the active damping control approach may not always provide better disturbance rejection in certain situations, depending on the present disturbance profiles.

### 5.2. Robustness to model uncertainty

A major drawback of the notch filter-based solution is its sensitivity to model uncertainties. The notch filter must be precisely tuned to the

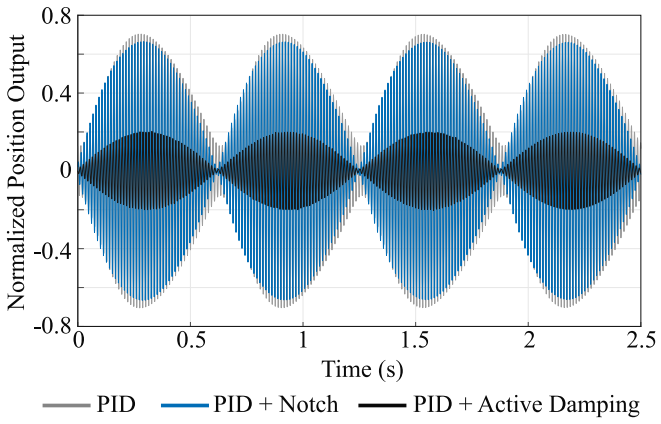


**Fig. 17.** Process disturbance rejection of multisine signal $d(t)$ for three comparison cases.

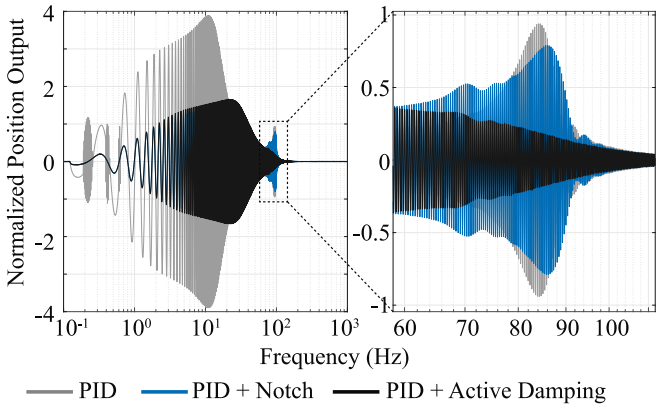


**Fig. 18.** Process disturbance rejection of chirp signal (0.1 Hz–1000 Hz) for three comparison cases.

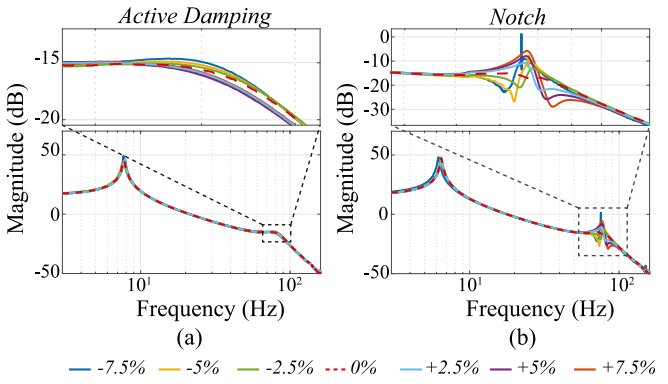


**Fig. 19.** Effectiveness of active damping control (a) and notch filter (b) under varying percentages of resonance frequency uncertainty.

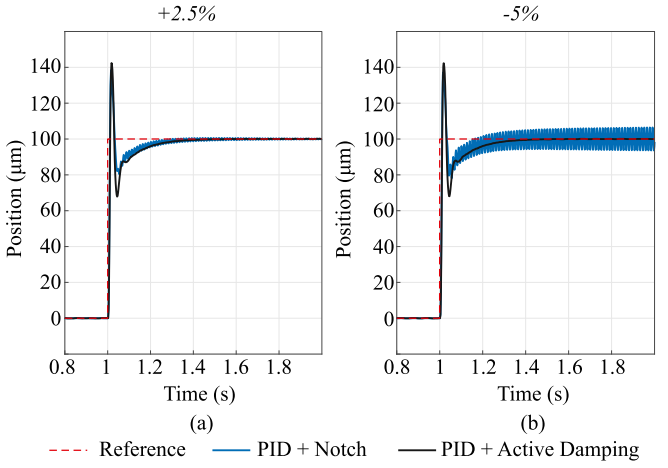


**Fig. 20.** Illustration cases of closed-loop step reference tracking with +2.5% (a) and −5% (b) of resonance frequency uncertainty $\delta$.

exact frequency of the delimiting resonance. Any deviation in the actual resonance frequency from the model can severely degrade the filter's performance, leading to increased disturbance errors, restricted control bandwidth, and potentially inducing instability.

In contrast, while the HP-PPF controller also requires alignment with the targeted resonance mode, it achieves damping through phase adjustment, as illustrated in Fig. 5, offering improved robustness against parameter variations. The notch filter mitigates the resonance by attenuating its gain, making it more susceptible to parameter variations. Although increasing the damping ratio of a notch filter can enhance robustness, it introduces additional phase lag, further restricting control bandwidth. Therefore, a trade-off exists between robustness to model uncertainty and control bandwidth in the case of a notch filter-based architecture, a trade-off that is significantly less pronounced with the novel active damping approach.

The experimental setup includes fixed resonance modes that cannot be easily modified. However, resonance mode uncertainty can be simulated by adjusting the frequency location of the HP-PPF controller and notch filter. The target frequencies of both controllers ($\omega_c$, $\omega_N$), which are typically set equal to the frequency of the target mode ($\omega_2$), are shifted by a factor $\delta$:

$$\hat{\omega}_c = \omega_2 + \delta \cdot \omega_2, \quad \hat{\omega}_N = \omega_2 + \delta \cdot \omega_2 \tag{31}$$

The impact of this added uncertainty on the performance of the active damping control architecture and the notch-based approach can be observed using closed-loop system identification. Fig. 19(a) presents the closed damping loop response ($CL_d(s)$) and Fig. 19(b) the open-loop notch response ($N(s) \cdot G(s)$) under different levels of resonance uncertainty. The results demonstrate the superior robustness of the active damping controller compared to the notch filter when faced with resonance mode uncertainty.

The closed-loop tracking responses to a step reference in Fig. 20 demonstrate that the control architecture with a notch filter tends towards instability as the mismatch between the notch frequency and the resonance grows. In contrast, the active damping controller maintains consistent performance, showing no signs of degradation under variations in the resonance frequency within the considered range.

## 6. Conclusion

This research introduces a novel active damping control method designed to suppress higher-order resonance modes in positioning systems. By incorporating a second-order high-pass filter within a positive feedback loop (HP-PPF), the approach specifically targets higher-order delimiting modes, which typically introduce unwanted vibrations and reduce positioning accuracy. The proposed method effectively enhances the damping characteristics of these undesired modes. To demonstrate the contributions of this work, the proposed active damping control is integrated into a dual-loop configuration that operates in parallel with a PID controller for tracking control. This configuration provides active damping for a non-collocated dual-stage positioning system, where the dominant non-collocated higher-order resonance not only contributes to disturbance errors but also significantly limits control bandwidth. Through simultaneous optimization of both the active damping and tracking controllers, the dual-loop architecture shows improved disturbance rejection at the frequency of the higher-order mode, as well

as enhanced robustness against model uncertainties, overcoming the limitations of traditional notch filters. The active damping control solution achieves an open-loop control bandwidth comparable to that of a notch filter-based architecture while providing better disturbance rejection and robustness against model uncertainties. A mathematical framework was developed to generalize these contributions, which were experimentally validated using a single-axis dual-stage compliant positioning system as a proof-of-concept setup.

Beyond the specific application studied, the HP-PPF method has broader applicability. By adjusting the feedback sign, it can also be used for active damping of higher-order collocated resonance modes. Additionally, for damping multiple modes, the method can be applied in parallel for each higher-order mode and integrated alongside existing techniques for primary mode damping. Further research should explore its applicability in systems with multiple degrees of freedom, where the HP-PPF method could be implemented in a decentralized architecture across different axes. Although the experimental implementation shows successful feedback noise attenuation with a second-order low-pass filter, optimizing the tuning of the low-pass filter frequency is recommended. This optimization should account for the trade-off between damping performance and noise attenuation, which can be achieved using methods like dynamic error budgeting, particularly when application-specific disturbances and noise profiles are known. Additionally, the observed increase in low-frequency process sensitivity due to the delimiting resonance peak reduction underscores the need for precise controller tuning based on application-specific disturbance rejection requirements. Furthermore, the impact of real-time system delays on phase properties and therewith damping performance must be addressed. Finally, a qualitative comparison with more complex existing control methods, such as modal control and $H_\infty$-synthesis, would provide valuable insights into the relative performance of the HP-PPF approach. Future investigations could focus on the broader application of this strategy to improve robustness and performance across various systems.

## CRediT authorship contribution statement

**N.J. Dee:** Writing – review & editing, Writing – original draft, Visualization, Validation, Software, Project administration, Methodology, Investigation, Formal analysis, Data curation, Conceptualization. **A.M. Natu:** Writing – review & editing, Writing – original draft, Visualization, Validation, Supervision, Methodology, Formal analysis, Conceptualization. **S.H. HosseinNia:** Writing – review & editing, Visualization, Validation, Supervision, Resources, Methodology.

## Declaration of competing interest

The authors declare that they have no known competing financial interests or personal relationships that could have appeared to influence the work reported in this paper.

## Data availability

Data will be made available on request.

## References


[1] Zhang Y, Zhao H, Zuo L. Contact dynamics of tapping mode atomic force microscopy. J Sound Vib 2012;331(23):5141–52.

[2] Wang F, Liang C, Tian Y, Zhao X, Zhang D. Design of a piezoelectric-actuated microgripper with a three-stage flexure-based amplification. IEEE/ASME Trans Mechatronics 2014;20(5):2205–13.

[3] Polit S, Dong J. Development of a high-bandwidth XY nanopositioning stage for high-rate micro-/nanomanufacturing. IEEE/ASME Trans Mechatronics 2010;16(4):724–33.

[4] Bronowicki AJ, Abhyankar NS, Griffin SF. Active vibration control of large optical space structures. Smart Mater Struct 1999;8(6):740.

[5] Liu Y, Deng J, Su Q. Review on multi-degree-of-freedom piezoelectric motion stage. IEEE Access 2018;6:59986–60004.

[6] Eielsen AA, Vagia M, Gravdahl JT, Pettersen KY. Damping and tracking control schemes for nanopositioning. IEEE/ASME Trans Mechatronics 2013;19(2):432–44.

[7] Holterman J. Vibration control of high-precision machines with active structural elements. 2002.

[8] Preumont A. In: Vibration control of active structures: an introduction, vol. 246, Springer; 2018.

[9] Devasia S, Eleftheriou E, Moheimani SR. A survey of control issues in nanopositioning. IEEE Trans Control Syst Technol 2007;15(5):802–23.

[10] Schitter G, Thurner PJ, Hansma PK. Design and input-shaping control of a novel scanner for high-speed atomic force microscopy. Mechatronics 2008;18(5–6):282–8.

[11] Butterworth JA, Pao LY, Abramovitch DY. Analysis and comparison of three discrete-time feedforward model-inverse control techniques for nonminimum-phase systems. Mechatronics 2012;22(5):577–87.

[12] Iwasaki M, Seki K, Maeda Y. High-precision motion control techniques: A promising approach to improving motion performance. IEEE Ind Electron Mag 2012;6(1):32–40.

[13] Gu G-Y, Zhu L-M. Motion control of piezoceramic actuators with creep, hysteresis and vibration compensation. Sensors Actuators A: Phys 2013;197:76–87.

[14] Tao Y, Li L, Li H-X, Zhu L. High-bandwidth tracking control of piezoactuated nanopositioning stages via active modal control. IEEE Trans Autom Sci Eng 2021;19(4):2998–3006.

[15] Natu A, Kaczmarek M, HosseinNia S. Overactuation for active damping in compliant positioning stage using piezoelectric transducers. IFAC-PapersOnLine 2024;58(7):269–74. http://dx.doi.org/10.1016/j.ifacol.2024.08.073, 4th IFAC Conference on Advances in Proportional-Integral-Derivate Control PID 2024.

[16] Kaczmarek MB, HosseinNia H. Fractional-order negative position feedback for vibration attenuation. Fractal Fract 2023;7(3):222.

[17] Kim S-M, Oh J-E. A modal filter approach to non-collocated vibration control of structures. J Sound Vib 2013;332(9):2207–21.

[18] Chomette B, Mamou-Mani A. Modal control based on direct modal parameters estimation. J Vib Control 2018;24(12):2389–99.

[19] Fedotov AV. Shape control and modal control strategies for active vibration suppression of a cantilever beam. In: International summer school-conference "advanced problems in mechanics". Springer; 2020, p. 234–44.

[20] Aphale SS, Ferreira A, Moheimani SR. A robust loop-shaping approach to fast and accurate nanopositioning. Sensors Actuators A: Phys 2013;204:88–96.

[21] Chen Z, Zhong X, Shi J, Zhang X. Damping-enabling technologies for broadband control of piezo-stages: A survey. Annu Rev Control 2021;52:120–34.

[22] Balas MJ. Direct velocity feedback control of large space structures. J Guid Control 1979;2(3):252–3.

[23] Aphale SS, Fleming AJ, Moheimani SR. Integral resonant control of collocated smart structures. Smart Mater Struct 2007;16(2):439.

[24] Fleming AJ. Nanopositioning system with force feedback for high-performance tracking and vibration control. IEEE/ Asme Trans Mechatronics 2009;15(3):433–47.

[25] Moheimani SR, Vautier BJ. Resonant control of structural vibration using charge-driven piezoelectric actuators. IEEE Trans Control Syst Technol 2005;13(6):1021–35.

[26] Goh C, Caughey T. On the stability problem caused by finite actuator dynamics in the collocated control of large space structures. Internat J Control 1985;41(3):787–802.

[27] Bhikkaji B, Ratnam M, Fleming AJ, Moheimani SR. High-performance control of piezoelectric tube scanners. IEEE Trans Control Syst Technol 2007;15(5):853–66.

[28] Li L, Li C-X, Gu G, Zhu L-M. Positive acceleration, velocity and position feedback based damping control approach for piezo-actuated nanopositioning stages. Mechatronics 2017;47:97–104.

[29] Dosch J, Leo D, Inman D. Modeling and control for vibration suppression of a flexible active structure. J Guid Control Dyn 1995;18(2):340–6.

[30] Kim S-M, Wang S, Brennan MJ. Comparison of negative and positive position feedback control of a flexible structure. Smart Mater Struct 2010;20(1):015011.

[31] Wang X, Li L, Zhu Z, Zhu L. Simultaneous damping and tracking control of a normal-stressed electromagnetic actuated nano-positioning stage. Sensors Actuators A: Phys 2022;338:113467.

[32] Das SK, Pota HR, Petersen IR. Damping controller design for nanopositioners: A mixed passivity, negative-imaginary, and small-gain approach. IEEE/ASME Trans Mechatronics 2014;20(1):416–26.

[33] Lanzon A, Petersen IR. Stability robustness of a feedback interconnection of systems with negative imaginary frequency response. IEEE Trans Autom Control 2008;53(4):1042–6.

[34] Song F, Liu Y, Dong Y, Chen X, Tan J. Motion control of wafer scanners in lithography systems: From setpoint generation to multi-stage coordination. IEEE Trans Instrum Meas 2024. http://dx.doi.org/10.1109/TIM.2024.3413202, 1–1.

[35] Zhu Z-H, Chen L, Niu Y, Pu X, Huang P, To S, et al. Triaxial fast tool servo using hybrid electromagnetic–piezoelectric actuation for diamond turning. IEEE Trans Ind Electron 2021;69(2):1728–38.
[36] HosseinNia SH, Saikumar N. Fractional-order precision motion control for mechatronic applications. Handb Fract Calc Appl 2019;6:339–56.
[37] Schmidt RM, Schitter G, Rankers A. The design of high performance mechatronics-: high-Tech functionality by multidisciplinary system integration. Ios Press; 2020.
[38] Nocedal J, Wright SJ. Numerical optimization. Springer; 1999.
[39] Monkhorst W. Dynamic error budgeting: A design approach. 2004.

**N.J. Dee**, graduated *cum laude* from the High-Tech Engineering track of the Mechanical Engineering M.Sc. programme at the Department of Precision and Microsystems Engineering, Delft University of Technology, Delft, The Netherlands, specializing in Mechatronics System Design.

**A.M. Natu** received the M.Sc. in Mechanical Engineering (*cum laude*) with a specialization in Mechatronics System Design and is currently employed as a Ph.D. Candidate at the Department of Precision and Microsystems Engineering, Delft University of Technology, Delft, The Netherlands. His research interests include active damping control, distributed actuation and sensing, precision mechatronics, and nanopositioning systems.

**S.H. HosseinNia** (Senior Member, IEEE) received the Ph.D. degree (Hons.) (*cum laude*) in electrical engineering specializing in automatic control: application in mechatronics from the University of Extremadura, Badajoz, Spain, in 2013. He has an industrial background, having worked with ABB, Sweden. Since October 2014, he has been appointed as a Faculty Member with the Department of Precision and Microsystems Engineering, Delft University of Technology, Delft, The Netherlands. He has co-authored numerous articles in respected journals, conference proceedings, and book chapters. His main research interests include precision mechatronic system design, precision motion control, and mechatronic systems with distributed actuation and sensing.